Polymer 218 (2021) 123492

Contents lists available at ScienceDirect

Polymer

journal homepage: http://www.elsevier.com/locate/polymer

# Photoresponsive thin films of well-synthesized azobenzene side-chain liquid crystalline polynorbornenes as command surface for patterned graphic writing

Jian Chen [a], Tianchi Xu [a], Weiguang Zhao [a], Ling-Ling Ma [b,**], Dongzhong Chen [a,*], Yan-Qing Lu [b]

[a] Key Laboratory of High Performance Polymer Materials and Technology of Ministry of Education, Collaborative Innovation Center of Chemistry for Life Sciences, Department of Polymer Science and Engineering, School of Chemistry and Chemical Engineering, Nanjing University, Nanjing, 210023, China
[b] National Laboratory of Solid State Microstructures, Key Laboratory of Intelligent Optical Sensing and Manipulation, College of Engineering and Applied Sciences, And Collaborative Innovation Center of Advanced Microstructures, Nanjing University, Nanjing, 210093, China

ARTICLE INFO

*Keywords:*
Azobenzene
Azopolymer
Command surface
Photoalignment
Ring-opening metathesis polymerization (ROMP)

ABSTRACT

Azobenzene-containing polymers (azopolymers) are a kind of intensively explored fascinating photoresponsive materials, liquid crystalline (LC) azopolymers with excellent film-forming, ordered structure and self-repairing capability are endowed with enhanced photoisomerization and photoalignment characteristics capable of developing into photo-modulated smart surfaces. Here in this work, two azobenzene side-chain LC polynorbornenes of PNB-Azo-n with different DP of $n = 50$ and 100 have been well synthesized through ring-opening metathesis polymerization (ROMP). The polynorbornene backbone of less flexibility with larger spacing between adjacent azobenzene side groups endows stronger inhibition for H-aggregation and better photoresponsiveness. The high-DP azopolynorbornene of PNB-Azo-100 thin films well behave as command surface for the upper layer nematic LC molecules thanks to their better performance in photoisomerization and photoalignment, together with their good compatibility and dissolution-resistance to the nematic LC mixture of E7. Selectively optically readable LC graphic writings at normal size through various photomasks have been demonstrated, and higher grid resolution up to sub-ten micrometer with a digital micromirror device (DMD) based dynamic photopatterning system has been achieved. Therefore, such kind of LC azopolynorbornenes demonstrate promising applications in LC photoalignment system and photoresponsive devices for potential anti-forgery document security and smart card technology.

## 1. Introduction

Azobenzene (Azo) is one of the most widely adopted and intensively explored multifunctional chromophore among various photochromic dyes and photoresponsive materials [1–7]. With the adoption of mesogenic Azo chromophores, thus constructed photochromic liquid crystalline (LC) materials are endowed with fascinating photoresponsive characteristics such as photoisomerization and photoalignment, serving as a promising platform for developing photo-modulated smart surfaces by virtue of long-range ordering, mobility, and response to light stimulation [8–11]. Upon irradiation with linear polarized light or non-polarized light, such Azo-based photochromic LC materials can achieve photoalignment according to the polarized direction or light propagation direction [8–11]. However, the occurrence of *trans-cis* photoisomerization needs sufficient free volume and the photoalignment of Azo chromophores requires even more free space for the involved motion of the whole chromophore moieties [8,9].

For low molecular weight (MW) azobenzene derivatives in solution, their photoisomerization is well demonstrated, while in the bulk state or in film, the photoisomerization, let alone photoalignment, is often significantly weakened or even completely hindered due to severe H-aggregation [8,9]. The motions induced by photoisomerization were classified into three types: at the molecular level, at the nanometer domain level, and at the micrometer macroscopic level [9]. When the

* Corresponding author.
** Corresponding author.
*E-mail addresses:* malingling@nju.edu.cn (L.-L. Ma), cdz@nju.edu.cn (D. Chen).

https://doi.org/10.1016/j.polymer.2021.123492
Received 3 December 2020; Received in revised form 26 January 2021; Accepted 28 January 2021
Available online 2 February 2021

Azo chromophores arranged in a side-by-side way mainly through dipolar interactions to form H-aggregation, photoisomerization and the first type of motion were badly suppressed thus would lose their photoresponsive capabilities. Various strategies have been employed for the realization of photoresponsive characteristics. On the one hand, introducing some charged groups, such as sulfonic group, into azobenzene chromophore can effectively suppress the H-aggregation in the bulk state, for instance, the typical low MW photoaligning agent of diazo-dye functionalized with sulphonic acid SD1 (sodium salt of 4,4′-bis (4-hydroxy-3-carboxy-phenylazo)- 2,2′-disulphonic acid biphenyl) [12,13]. Yet modified with charged groups usually resulted in low solubility in organic solvent, and the poor film-forming capability of low MW dyes seriously limited their applications. On the other hand, azobenzene dendritic LC systems exhibited substantially accelerated photoisomerization through diluting the azobenzene content with azobenzene-aliphatic codendron method to effectively inhibit the formation tendency of H-aggregation [14,15]. Moreover, macrocyclic effects seemed to work well by introducing a semi-rigid framework with a cavity to offer sufficient free volume. Such as the early impressive work reported by Ichimura and coworker of calixarene-based macrocyclic amphiphiles with Azo units elaborately demonstrated a photoresponsive surface showing photo-triggered contact angle change and light-driven directional motion of a liquid droplet on the surface [16,17]. We presented the first example of multi-azobenzene modified pillar [5]arene macrocyclic compound showing wide temperature range smectic LC mesophase and the tubular macrocyclic framework providing sufficient free volume for azobenzene moieties to achieve reversible photoisomerization and photoalignment, thus endowed their thin films with excellent light-driven modulation of surface free energy, wettability, and even photoalignment-mediated orientation of discotic columnar LC mesophase [18]. Nevertheless, the synthesis of macrocyclic derivatives, especially for functionalized asymmetrically substituted systems, was very time-consuming and laborious, thus faced great challenges in scale-up synthesis and limited their potential applications.

So far, the introduction of azobenzene into polymers has been proved to be a very effective strategy among others, where azobenzene-containing polymers (azopolymers) have been intensively explored [8–11,19–40], which revealed quite promising thanks to the free volume introduced by the polymer backbone and excellent film-formation and self-repairing capability of the LC azopolymer films to keep from the possible damage in multiple photoisomerization or photoalignment cycles. Especially LC azopolymers, which were pioneered by Ikeda and coworkers [10,11,34,36–38] with the Azo chromophores acted both as mesogenic units in their *trans* form and as photoresponsive groups, demonstrated as versatile light-responsive materials in their bulk state or thin films based on reversible photoisomerization or photo-induced alignment [9–11,19–22,24–40], or even achieved the photoinduced alignment of PEO nanocylinders *via* nanoscale supramolecular cooperative motions in the Azo-based LC block copolymers with poly (ethylene oxide) (PEO) block introduced [35–40].

Furthermore, the interface of the assembled systems or film surface based on such kind of LC azopolymers or copolymers manifested molecular amplification of surface-assisted photoalignment regulating the orientation of up-layer mesogens, serving as "command surface" as first proposed and intensively explored by Ichimura group [8,41–45] and by Seki and coworkers [46–53].

However, almost all the reported azopolymers or copolymers applied for photoresponsive interfaces were based on relatively flexible backbone of poly(meth)acrylate [8–11,26,30–40,44,52,53], or derived from poly(vinyl alcohol) as the interface model of the command surface system [46–51], except few examples with the less flexible or semi-rigid polynorbornene backbone [54–56]. Although it is believed that the backbone flexibility, degree of polymerization (DP), the substitution density of side groups and the side-chain spacer length have important effects on its surface-assisted photoalignment and command surface capabilities [42,46–53], while how these factors take effect still remains great challenging with many questions not well addressed.

The excellent controllability and readily realization of high-MW functional polymers constituted popular characteristics of ring-opening metathesis polymerization (ROMP) [28,54–56], which provided a good synthesis pathway for the preparation of photoresponsive side-chain azopolymers. Herein we present the preparation of side-chain LC azopolymers with polynorbornene backbone *via* ROMP. Two well-synthesized azobenzene side-chain liquid crystalline polynorbornenes with different DP have been prepared. For the functionalized norbornene monomer, the introduction of azobenzene mesogen through the imide linkage rather than directly attached to the aliphatic ring avoided the complexity resulting from different substitution positions on the ring [57], and the adoption of polynorbornene backbone of larger spacing and less flexibility was beneficial for inhibiting H-aggregation of Azo group and presenting better photoresponsiveness. The selection of polynorbornene backbone of moderate semi-rigidity with a suitable side-chain substitution density showed reasonable for the photoresponsive azopolymers, which was somehow reminiscent of the conclusion obtained for the side-chain discotic LC polymers based on the dissipative particle dynamics (DPD) simulation method in our very recent report that a moderate grafting density, a backbone of sufficient length and proper flexibility was preferred [58], acting as a certain contrast reference. After comparative investigation of the two azobenzene side-chain LC polynorbornenes of different DP on their structures, thermal and photo-responsive behaviors, the thin films of high-DP Azo-polynorbornene were employed as photoalignment regulated command surface for nematic liquid crystal E7 [59], enabling graphic writing at normal size through conventional photomask or even reaching resolution below 10 μm with adopting a dynamic photopatterning system based on digital micromirror device (DMD) [13,60–62], demonstrating promising applications for potential anti-forgery document security and smart card technology.

## 2. Experimental section

### 2.1. Materials and characterization

The reagents phenol (99%), ammonium acetate ($NH_4OAc$, 98%), acetic acid (AcOH, 99.5%), concentrated hydrochloric acid (37 wt%), sodium hydroxide (NaOH, 96%), potassium carbonate ($K_2CO_3$, 99%), potassium iodide (KI, 99%), and sodium nitrite ($NaNO_2$, 99%) were purchased from Sinopharm Chemical Reagent Company. 1-Bromodecane (98%), and 1,10-dibromodecane (99%) were bought from TCI. 4-Acetamino phenol (99%) was purchased from Aladdin company. The *cis*-5-norbornene-*exo*-2,3-dicarboxylic anhydride (98%) was purchased from Bidepharm company. The 2nd Grubbs' catalyst (95%) was purchased from Innochem company. The nematic liquid crystal E7 is a commercial eutectic liquid crystal mixture mainly composed of *p*-alkyl or alkoxy cyanobiphenyl and cyanotriphenyl ($n_e = 1.741$, $n_0 = 1.517$, at 589 nm; $T_m = -40\ ^\circ C$, $T_{NI} = 59\ ^\circ C$; from Suzhou King Optonics Co. Ltd). The solvent trichloromethane was distilled from calcium hydride ($CaH_2$) under reduced pressure before use. The solvents of *N,N*-dimethylformamide (DMF), tetrahydrofuran (THF), acetone, toluene, petroleum ether, and dichloromethane (DCM) were all of commercial reagents in AR grade and used as received without further purification.

All the $^1H$ NMR spectra were collected from a Bruker DPX 400 MHz nuclear magnetic resonance (NMR) spectrometer in $CDCl_3$ at 25 °C using tetramethylsilane (TMS) as the internal standard. Electrospray ionization mass spectra (ESI-MS) were obtained on LCMS-2020 single quadrupole mass spectrometer (Shimadzu). The number-average molecular weight ($M_{n,GPC}$) and molecular weight distribution ($M_w/M_n$) of the resultant polymers were determined using a Viscotek gel permeation chromatography (GPC) instrument (Model: TDAmax) equipped with a differential refractive index detector (TDA305), using TGard, T4000, and T2500 columns with measurable molecular weight ranging from $5 \times 10^2$ to $5 \times 10^5$. The chromatographically pure THF was employed as

the eluent at a flow rate of 1.0 mL/min at 35 °C. GPC samples were filtered over a filter of pore size 0.22 μm, injected by a Malvern autosampler and calibrated with polystyrene (PSt) standard. UV–vis spectra for solution or film samples were recorded using a Shimadzu UV3600 spectrophotometer. Differential scanning calorimetry (DSC) thermograms were recorded on a Mettler-Toledo DSC1 at a heating or cooling rate of 10 °C/min under nitrogen atmosphere. Typically, about 8 mg sample was encapsulated in a sealed aluminum pan with an identical empty pan as the reference, and indium was used as a calibration standard. Polarized optical microscopy (POM) investigations of thermal transition behaviors were performed with a PM6000 microscope under cross-polarizers equipped with a Leitz-350 heating stage. The texture photographs were captured using an associated Nikon (D3100) digital camera. X-ray scattering experiments were performed with a high-flux small-angle X-ray scattering instrument (SAXSess mc$^2$, Anon Paar) equipped with Kratky block-collimation system and a temperature control unit. Both SAXS and WAXS were simultaneously recorded on an imaging plate (IP) that extended to high-angle range (the $q$ range covered by the IP was from 0.06 to 29 nm$^{-1}$, $q = 4\pi\sin\theta/\lambda$, where the wavelength $\lambda$ is 0.1542 nm of Cu-K$\alpha$ radiation and $2\theta$ is the scattering angle) at 40 kV and 50 mA. Typically, the powder sample was encapsulated with aluminum foil during the measurement and the obtained X-ray analysis data were processed with the associated SAXSquant software 3.80 (supplied by Anton Paar GmbH). To eliminate the thermal history influence, all the polymer samples for SAXS/WAXS tests experienced a melting procedure firstly and then cooled down from the isotropic state to the preset temperature. The thin films of Azo side-chain polynorbornenes were fabricated with typically a 5 wt% polymer solution in toluene through spin-coating on indium-tin oxide (ITO) glass or quartz substrates (2.0 cm × 1.5 cm) using a spin coater (CHINAPONY KW-8A) at 800 r/min. The depth of the surface profile was recorded at room temperature with a Bruker DektakXT profilometer in a tapping mode. Contact angle (CA) measurements were performed with a KSV CAM200 optical contact angle analyzer. A 3 μL olive oil droplet was carefully deposited on the film surface, and the pristine digital image of the drop profile was collected about 5 s after the drop contact. The ambient temperature and humidity during the measurements were 25 °C and 50%, respectively. The contact angle is the average value of at least three independent measurements in different regions of the investigated film sample. The 365 nm UV light or 450 nm visible light irradiation was generated from Hg–Xe lamp (CHF-XM500W power system, China) at 30 °C through the corresponding band-pass filter. The DMD based dynamic photoalignment system was assembled from multiple parts, mainly including a mercury lamp (S1000, EXFO, Canada) filtered between 320 and 500 nm for the generation of a uniform and collimated light beam, a digital mirror (1024 × 768, Discovery 3000, Texas Instruments) device as a dynamic mask consisting of more than 78,600 micromirrors, an apochromatically corrected projection lens (10 × , NA = 0.3, WD = 34 mm, Conv Optics Co., China) as an image focusing part, an image plane to record the alignment information, as well as a CCD device to monitor the focusing process of the image.

### 2.2. Synthesis of Azo norbornene monomer MNB-Azo

The detailed synthetic procedure of the monomer MNB-Azo is provided in the Supporting Information together with characterization results for all the intermediates, the Azo norbornene monomer MNB-Azo was harvested in a separated yield of 45.0%, with the $^1$H NMR spectrum presented in Fig. 1a. $^1$H NMR (400 MHz, $CDCl_3$): δ 8.06 (d, 4H), 7.01 (d, 4H), 6.28 (t, 2H), 4.05 (t, 4H), 3.46 (t, 2H), 3.27 (t, 2H), 2.67 (d, 2H), 1.87–1.76 (m, 2H), 1.60–1.19 (m, 32H), 0.89 (t, 3H). ESI-MS ($m/z$): [M + H]$^+$ calcd. for $C_{41}H_{58}N_3O_4$, 656.93; found, 656.35.

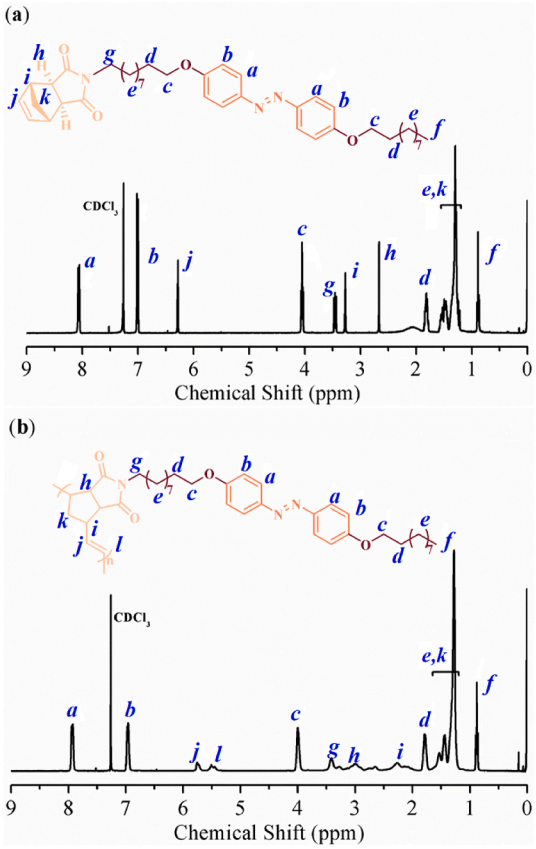


**Fig. 1.** $^1$H NMR spectra comparison of (a) the monomer MNB-Azo, and (b) the DP 50 polymer PNB-Azo-50 in $CDCl_3$ at room temperature.

### 2.3. Preparation of Azo side-chain polynorbornenes PNB-Azo-n with different DP of n = 50, 100 through ROMP

The typical polymerization procedure for the preparation of polynorbornenes with Azo side-chain is described here for PNB-Azo-50 of DP $n = 50$. The monomer MNB-Azo (200.0 mg, 0.31 mmol), lab-made 3rd generation Grubbs' catalyst (see Scheme S2, 4.6mg, 6.3 × 10$^{-3}$ mmol), and anhydrous trichloromethane (1.5 mL) were added into a round-bottom Schlenk flask (10 mL) equipped with a magnetic stirring bar. The reaction mixture was degassed for at least three freeze-pump-thaw cycles to ensure a high purity inert nitrogen atmosphere. Then the ROMP reaction was carried out at room temperature (25 °C) under stirring for 3 h. The reaction was terminated by addition of ethyl vinyl ether and then the reaction mixture was transferred with trichloromethane (~2 mL) to precipitate into a large amount of cold methanol (~200 mL). Finally, the solid precipitate product was filtered, washed with methanol and dried at 35 °C under reduced pressure in a vacuum oven until constant weight, 140.4 mg pale yellow solid product PNB-Azo-50 was harvested in yield 70.2%.

$^1$H NMR (400 MHz, $CDCl_3$) for PNB-Azo-50 (see Fig. 1b): δ 7.93 (d, 4H, **a**), 6.96 (d, 4H, **b**), 5.80–5.67 (d, 1H, **j**), 5.58–5.39 (d, 1H, **l**), 4.00 (t, 4H, **c**), 3.51–3.20 (m, **g**), 3.17–2.85 (m, **h**), 2.43–1.97 (m, **i**), 1.85–1.71 (m, 4H, **d**), 1.68–1.15 (m, **e,k**), 0.88 (t, 3H, **f**).

The DP 100 polymer of PNB-Azo-100 was similarly prepared with the feed ratio $[MNB\text{-}Azo]_0$: $[Cat]_0 = 100 : 1$ and collected with a yield of 78.6%. $^1$H NMR spectrum for PNB-Azo-100 is provided in the supporting information (see Fig. S6).

### 2.4. Fabrication of PNB-Azo-n ($n = 50, 100$) polymer thin films on various substrates via spin-coating

In most cases, the thin films were fabricated through spin-coating of a 5 wt% toluene solution of the polymer PNB-Azo-n with $n = 50$ or 100 on ITO-coated glass substrates, or on quartz substrates for those prepared for UV–vis tests. The purchased ITO-glass was first cleaned for 1 h in a sonic bath with surfactant added, after rinsed with deionized water, acetone, and isopropyl alcohol in sequence, then dried in an oven at 100 °C for 1 h. All the spin-coated polymer films were completely dried at 65 °C for 10 min with the film thickness measured with the profilometer to be at around 180 nm, besides for those LC polymer films in periodic stripe patterns, relatively thicker films (~300 nm) were fabricated from 10 wt% solution of the corresponding polymer in toluene to enhance the birefringence contrast and facilitate observation of the POM textures.

### 2.5. Photoalignment of high-DP Azo-polynorbornene thin films of PNB-Azo-100 and photomask-assisted patterned films as command surface

The spin-coated thin films of PNB-Azo-100 was irradiated through a photomask with 365 nm UV light or 450 nm visible light in an adjustable incident angle to prepare the designed surface. The optical birefringence change of the photoaligned patterns was confirmed and investigated with POM and the patterned films was further employed as command surface for pattern reproduction with nematic liquid crystal E7.

### 2.6. Programmable photoalignment of PNB-Azo-100 thin films via the DMD based micro-lithography system

The digital micromirror device (DMD)-based microlithography system [60] was employed for the programmable photoalignment of PNB-Azo-100 thin films. The PNB-Azo-100 thin film on the ITO-glass substrate was firstly irradiated with blue light ($\lambda = 450$ nm) at a tilt angle of 60° incident with respect to the film surface. The obliquely photo-aligned thin film was then placed on the object stage of the DMD system, and subsequently exposed to the light beam (energy density: 5.0 J/cm$^2$), which has been patterned by the computer-modulated on/off state of each micromirror in the digital mirror chip (1024 × 768 micromirror array). The second photoalignment using the DMD system was conducted to achieve a multi-dimensional and multi-domain photoaligned surface in a sub-ten-micrometer resolution, which subsequently acted as a command surface. Afterwards, the nematic liquid crystal E7 was spin-coated at a low rate on the pre-aligned film as the upper layer to accomplish the preparation of a composite film of E7/PNB-Azo-100. Then the optical birefringence images and changes of thus obtained composite films were monitored by POM investigation at room temperature.

## 3. Results and discussion

### 3.1. Synthesis and characterization of azobenzene side-chain polynorbornenes

The synthesized Azo-norbornene monomer MNB-Azo was then polymerized *via* the ROMP method with the 3rd generation Grubbs' catalyst at room temperature. As summarizaed in Table 1, the polymerization progressed well in a separated yield more than 70% for both Azo side-chain polynorbornenes of PNB-Azo-n with DP $n = 50$ or 100. It is revealed that the theoretical molecular weight ($M_{n,th}$) estimated from the feed ratio of $[MNB\text{-}Azo]_0/[Cat]_0$ agreed well with the number-average molecular weight determined from GPC measurements ($M_{n,GPC}$), and a relatively narrow polydispersity index (PDI) was achieved, manifesting good controllability of ROMP technique for the norbornene monomer with an imide-linked azobenzene side group. Moreover, as anticipated the GPC measured number-average molecular weight of $M_{n,GPC} = 49{,}200$ for PNB-Azo-100 was rather precisely twice of that for PNB-Azo-50 with $M_{n,GPC} = 24{,}100$.

**Table 1**
The polymerization and molecular characterization results of the Azo side-chain polynorbornenes of PNB-Azo-n *via* ROMP with DP $n = 50$ and 100.

| Polymer code | Feed ratio | Yield (%) | $M_{n,th}$ | $M_{n,GPC}$ | PDI |
|---|---|---|---|---|---|
| **PNB-Azo-50** | 50:1 | 70.2 | 23,000 | 24,100 | 1.35 |
| **PNB-Azo-100** | 100:1 | 78.6 | 51,600 | 49,200 | 1.47 |

The $^1$H NMR spectra comparison of the monomer MNB-Azo and the polymer PNB-Azo-50 corroborated the changes before and after polymerization and confirmed their composition and structures. As shown in Fig. 1b, the broadened peaks of all the signals in the PNB-Azo-50 spectrum as compared to those of the monomer in Fig. 1a indicated the typical polymer spectroscopic feature. More specifically, there were only insignificant changes on the chemical shifts and relative intensities for all those hydrogen protons in the side chain of aromatic azobenzene core and aliphatic alkyl tail or spacer denoted as from ***a*** to ***g***. While those proton signals from ***h*** to ***l*** in the polymer revealed obvious changes both in chemical shifts, symmetries and relative intensities as compared to those from ***h*** to ***k*** belonging to the unopened cyclical norbornene moiety in the monomer, confirming the occurrence of ring-opening metathesis polymerization into polynorbornene backbone and can be well assigned as provided in the experimental section.

### 3.2. Thermal behaviors and lamellar smectic LC phase structures of PNB-Azo-n ($n = 50, 100$)

The thermal properties and phase transition behaviors of the azobenzene side-chain polynorbornenes of PNB-Azo-n ($n = 50, 100$) were investigated with DSC and POM, and their structures were explored together with SAXS/WAXS. As shown in Fig. 2b, both polymers exhibited clearly a glass transition temperature ($T_g$) and an isotropization temperature ($T_{iso}$) in both heating and cooling scan cycles, together with their grainy textures as revealed by POM investigation (Fig. S10), manifesting an enantiotropic LC phase behavior. It is not unexpected that the $T_g = 56.8$ °C of the high-DP polymer PNB-Azo-100 was several degrees higher than that of 52.6 °C for PNB-Azo-50 determined from the second heating scan, while on the contrary, the $T_{iso} = 114.9$ °C for the low-DP polymer PNB-Azo-50 was slightly higher than that of 112 °C for PNB-Azo-100. Moreover, as summarized in Table 2, the enthalpy changes of isotropization significantly increased for PNB-Azo-50 in either heating or cooling scans as compared to those for PNB-Azo-100. Such a seemingly somewhat anomalous performance in isotropization temperatures and enthalpy changes, reflected the closer packing of Azo moieties in the low-DP polymer of PNB-Azo-50, which would be further discussed next together with SAXS/WAXS analysis results.

Variable temperature SAXS/WAXS studies provided more detailed and some quantitative structure information about the LC polynorbornenes of PNB-Azo-n ($n = 50, 100$). As shown in Fig. 2c and d, the sharp reflections in the small-angle region up to three orders characterized with $q$ ratio of 1:2:3 suggested an lamellar packing structure with layer spacings of 4.87 nm for PNB-Azo-50 and 4.98 nm for PNB-Azo-100 at 65 °C, which are larger than the stretching molecular contour length of 3.82 nm calculated with Chem3D, but smaller than twice the length, together with the broad halo at around 0.43 nm characteristic of alkyl average distance, indicating a smectic A mesophase (SmA) in interdigitated arrangement as depicted schematically as the insets in Fig. 2c and d. As summarized in Tables S1 and S2 in the Supporting Information, the layer spacings exhibited slightly increasing upon heating and manifested a frozen smectic LC phase upon cooling down to room temperature at 25 °C with reduced spacings. It is interesting to note that the full-width at half-maximum (FWHM) of scattering peaks in the small-angle region for PNB-Azo-100 was broader than that for PNB-Azo-50, and the FWHMs of characteristic scattering peaks of such azopolymers with

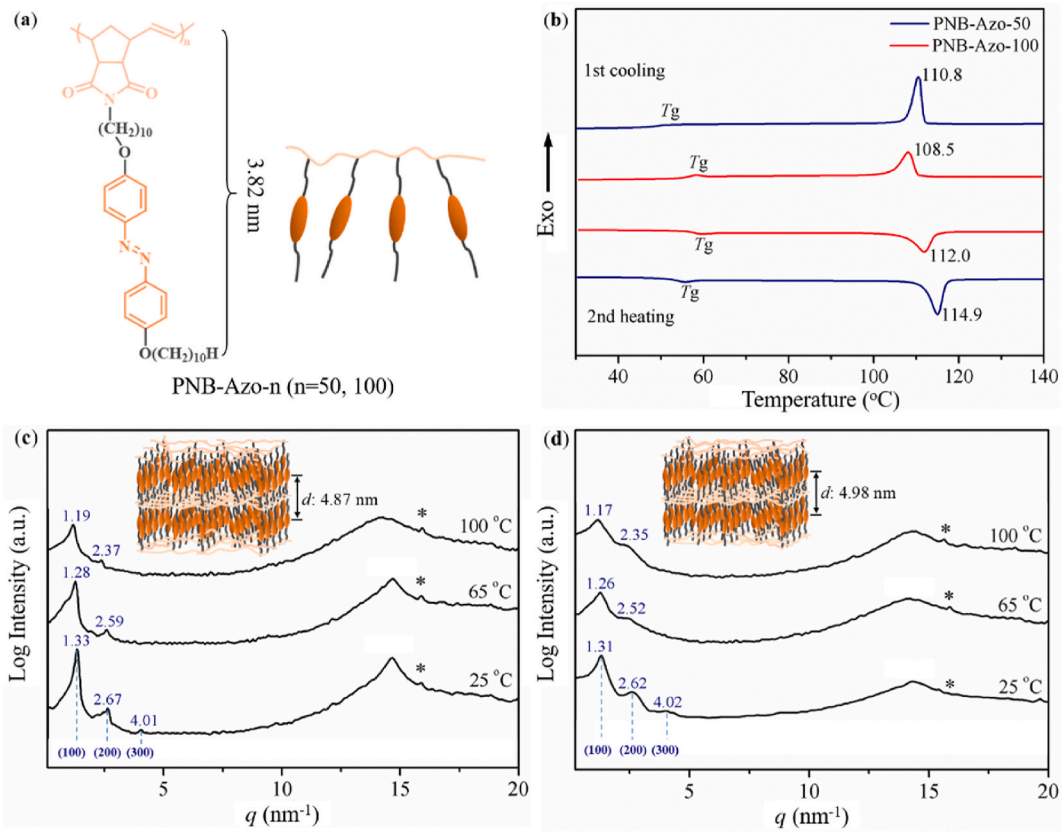


**Fig. 2.** (a) Chemical structures and schematic illustrations of Azo side-chain polynorbornenes PNB-Azo-n ($n$ = 50, 100). (b) DSC curves of PNB-Azo-n ($n$ = 50, 100) during the first cooling and second heating scans at a rate of 10 °C/min under nitrogen atmosphere. SAXS/WAXS profiles of (c) PNB-Azo-50, and (d) PNB-Azo-100 at selected temperatures of 25 °C, 65 °C, and 100 °C, with the inset cartoons schematically illustrating the smectic lamellar structures labelled with the layer spacing at 65 °C. *The background peaks from the packing aluminum foil lying in the wide-angle region are marked with asterisks, which have a negligible disturbance to the interested sample peaks thus without complete subtraction so as to avoid distorting the peak shape and smoothing over some significant weak signals.

**Table 2**
Thermotropic transition temperatures and associated phase assignments for the azobenzene side-chain LC polynorbornenes of PNB-Azo-n ($n$ = 50, 100).

| Polymer code | Transition temp. °C (Enthalpy change, J/g)[a] | | $d$ [c] (nm) |
|---|---|---|---|
| | Second heating[b] | First cooling[b] | |
| **PNB-Azo-50** | G 52.6 SmA 114.9 (4.02) Iso | Iso 110.8 (4.22) SmA 51.2 G | 4.87 |
| **PNB-Azo-100** | G 56.8 SmA 112 (2.93) Iso | Iso 108.5 (2.68) SmA 56.2 G | 4.98 |

[a] G, glass state; SmA, smetic A phase; Iso, isotropic state.
[b] With heating or cooling rate of 10 °C/min.
[c] The LC layer spacing of SmA at 65 °C determined from SAXS/WAXS analysis.

polynorbornene backbone were relatively broader than those with poly (meth)acrylate main chain [5,7,26,33,52,53], which indicated the looser packing of the side-chain Azo chromophores and the poorer ordering of the smectic layer structure for the azopolymers with semi-rigid polynorbornene backbone, being yet favorable for photo-response. Furthermore, the much sharper and stronger peak centered at around $q$ = 14.66 $nm^{-1}$ in the lower temperature region for the low-DP polymer of PNB-Azo-50 (eg. at 25 °C, 65 °C, Fig. 2c) as compared to that for PNB-Azo-100, together with the reduced layer spacing, indicated a more compact and closer packing in PNB-Azo-50, in well accordance with its promoted isotropization temperature from DSC investigation, which thus more strongly inhibited the photoisomerization of Azo moieties and weakened the photoresponsive performance of the low-DP azopolymer of PNB-Azo-50 as discussed next.

### *3.3. Photoisomerization of azobenzene side-chain polynorbornenes of PNB-Azo-n ($n$ = 50, 100)*

The UV–vis spectra comparison of the monomer MNB-Azo and the Azo-polynorbornenes of PNB-Azo-n ($n$ = 50, 100) is provided in the Supporting Information (Fig. S9). The characteristic absorption peaks in the UV–vis spectra for both the monomer MNB-Azo and polymer PNB-Azo-n ($n$ = 50, 100) in the solution state were the same at around 359 nm (Fig. S9a), which were attributed to the π-π* absorption of Azo chromophores in their thermal-stable *trans* state. Whereas in sharp contrast, MNB-Azo, PNB-Azo-50 and PNB-Azo-100 in the thin film solid state obtained *via* spin-coating 5 wt% toluene solutions on quartz plates exhibited quite different absorption behaviors with the absorption peaks at 316 nm, 339 nm, and 342 nm, respectively (Fig. S9b). From the solution state to the solid film, the large hypsochromic shift of more than 40 nm for the monomer of MNB-Azo indicated the severe H-aggregation of Azo chromophores in the bulk solid state monomer. On the contrary, the quite modest hypsochromic shift of not exceeding 20 nm manifested significantly weakened H-aggregation effect in the case of Azo-polynorbornene polymers of PNB-Azo-n ($n$ = 50, 100). For exploring the photoresponsive capability of PNB-Azo-n ($n$ = 50, 100) enhanced by the macromolecular structure design, the reversible *trans-cis* photo-isomerization of the azopolymers as compared with the monomer in their thin film solid state was investigated and monitored with UV–vis spectroscopy. The intensity of the characteristic absorption band with peak at around 340 nm for both polymers (Fig. 3a and b), attributed to the π-π* transition of azobenzene *trans* isomer, decreased gradually under 365 nm UV light irradiation, along with intensity increase of the shoulder peak at around 460 nm characteristic of n-π* transition of

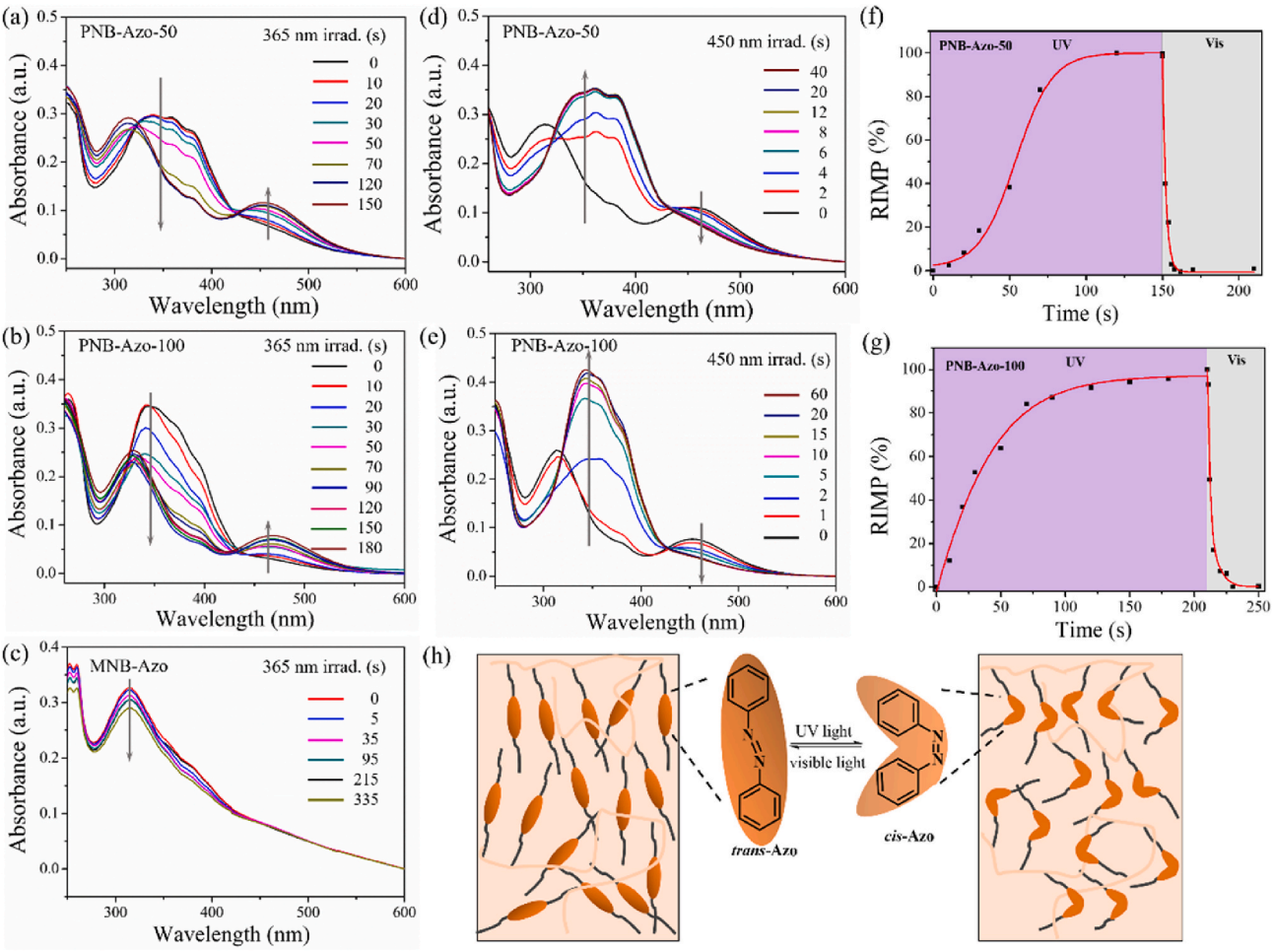


**Fig. 3.** UV–vis absorption spectra evolution of thin films on quartz substrates of (a) PNB-Azo-50, (b) PNB-Azo-100, and (c) MNB-Azo, under 365 nm UV light irradiation through *trans-cis* transition, and (d) PNB-Azo-50, (e) PNB-Azo-100 under 450 nm visible light irradiation successively after reaching the photostationary state. Plots of relative isomerization percentage (RIMP, %) versus the irradiation time for thin films of (f) PNB-Azo-50, and (g) PNB-Azo-100. (h) Schematic illustration of reversible *trans-cis* photoisomerization in the solid state thin films of PNB-Azo-n ($n = 50, 100$) under irradiation of different wavelength (365 nm UV or 450 nm visible light).

azobenzene *cis* isomer, whereas in sharp contrast the UV–vis absorption spectra for the monomer MNB-Azo thin film showed insignificant changes even under long time irradiation with 365 nm UV light (Fig. 3c), ascribing to severe H-aggregation effect.

Then under successive illumination with a 450 nm visible light after reaching the photostationary state under 365 nm UV light illumination, the absorption spectra both for PNB-Azo-50 (Fig. 3d) and PNB-Azo-100 (Fig. 3e) recovered to the initial state with a slightly increased intensity upon achieving thermal steady state through *cis-trans* transition. The different *trans-cis* transformation rate, as well as the variant irradiation time required to finish the reversible *trans-cis-trans* photoisomerization cycle of Azo chromophores in PNB-Azo-50 and PNB-Azo-100 reflected a significant impact of molecular weight on the photoresponsive performance of PNB-Azo-n ($n = 50, 100$). Here we define the relative isomerization percentage (RIMP) of *trans-cis* photoisomerization as determined from the following equation:

$$\text{RIMP}\ (\%) = 100 - I_x/I_{max} \times 100$$

Where $I_x$ stands for the instant peak absorption intensity and $I_{max}$ for the maximum peak absorption intensity of the characteristic absorption band with peak at around 340 nm. Then RIMP (%) is plotted as a function of the irradiation time for PNB-Azo-50 and PNB-Azo-100 thin films as shown in Fig. 3f and g, respectively. By comparison, it can be seen that PNB-Azo-100 showed a larger and more significant change in absorption intensity evolution resulted from photoisomerization in the solid state than PNB-Azo-50 did when compared Fig. 3b with 3a and Fig. 3e with 3 d. Moreover, it is revealed that upon irradiation with 365 nm light, PNB-Azo-50 exhibited an induction period of about 20 s to start up the photoisomerization (Fig. 3f), while PNB-Azo-100 responded quickly with RIMP increasing steadily before 90 s and then gradually leveling off with prolonged irradiation time (Fig. 3g). Overall, the combination of a semi-rigid polynorbornene backbone and a flexible ten-methylene spacer in PNB-Azo-n ($n = 50, 100$) created an appropriate micro-environment with sufficient free volume for the occurrence of reversible *trans-cis-trans* photoisomerization of Azo chromophores and endowed the azopolynorbornenes with desired photoresponsiveness in the solid state as schematically shown in Fig. 3h. The high-DP azopolymer of PNB-Azo-100 exhibited more significant and quicker photoresponse, in consistent with its more favorable packing structure providing larger free volume as revealed by DSC and SAXS/WAXS analyses, together with its dissolution-resistance capability in E7 liquid crystal by comparison with PNB-Azo-50 as discussed next, thus PNB-Azo-100 was chosen for further surface properties examination and constructing command surface thin films for patterned graphic writing.

### 3.4. Manipulating solid film surface properties of the side-chain azopolynorbornene through trans-cis photoisomerization

Oil droplet contact angle (CA) tests were carried out to monitor the changes of the thin film surface properties manipulated by light irradiation. The surface free energy (SFE) of azopolymer films usually varied with the *trans-cis* photoisomerization of Azo chromophores transformed from the extended rod-like *trans*-form mesogens into bent *cis*-isomer units, and vice versa [8]. The film of PNB-Azo-100 of thickness about 300 nm on glass substrate was spin-coated from a 10 wt% toluene solution. After exposed to vertically incident 450 nm visible light for 1 h to ensure the homeotropic orientation of Azo chromophores, a droplet of olive oil (3 μL) was carefully deposited on the pre-oriented film surface, and the digital image was captured about 5 s after dripping to obtain CA = 29.8° (Fig. 4a). Then exposed to 365 nm UV light, the CA values decreased with visible spreading of the oil droplet on the film surface gradually with the increase of UV light irradiation time (Fig. 4b–e), reaching a minimum CA value of 13.2° after irradiation for 360 s (Fig. 4e), manifesting a slight increase of SFE for the PNB-Azo-100 thin film due to *trans-cis* photoisomerization. After a successive exposure of vertically incident 450 nm visible light for 1 h to induce the *cis* to *trans* back isomerization, the CA value increased to 20.2° (Fig. 4f). This experiment of CA change under UV/visible light illumination was carried out in situ after dripping the olive oil droplet, the reason why the CA value did not fully recover might be various. It is probable that the back isomerization under 450 nm visible light illumination did not completely occur due to the interactions between the side-chain alkyl tails and aliphatic oil component with oil droplet covered, and the non-ignorable weight of the oil droplet itself might also have a certain effect on the stretching recovery of Azo side groups.

### 3.5. Fabrication of periodic striping pattern surfaces of the side-chain azopolymer through mask-mediated photoalignment

As demonstrated above the azopolynorbornene thin film showed excellent photoresponse, thus we first tried to realize the photoalignment of PNB-Azo-100 thin films simply by changing the incident direction of 450 nm visible light with the help of a banded grating mask A as schematically illustrated in Fig. 5a. The spin-coated PNB-Azo-100 thin film was exposed to the vertically incident 450 nm light for 30 min to induce the homeotropic alignment of Azo units, and followed by irradiated with 450 nm light through a mask A for 1 h at an incident angel of 45° with the projection of the oblique light in parallel with the longitudinal axis of the banded grating mask to induce the oblique alignment of Azo units within the exposed stripe regions.

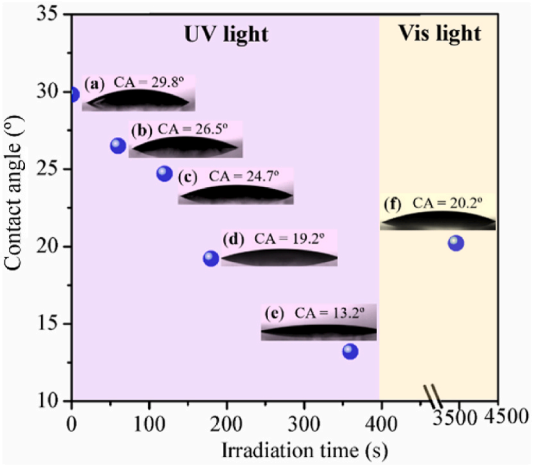


**Fig. 4.** Evolution of contact angle of PNB-Azo-100 thin film versus light irradiation time under 365 nm UV irradiation for (a) 0 s, (b) 60 s, (c) 120 s, (d) 180 s, (e) 360 s, and then under 450 nm visible light irradiation for (f) 3600 s, with the insets showing the oil droplet images.

The orientation character and alignment direction of the photoaligned PNB-Azo-100 thin films were investigated and corroborated with polarized optical microscopy (POM). As shown in Fig. 5b and c, upon rotating the sample stage, the stripes covered by the mask always remained as a dark field, indicating homeotropic orientation of Azo chromophores therein directed by the initial vertically incident light, while the stripes exposed to the obliquely incident light underwent a periodic transformation from dark field to bright field every 45°, which implied that Azo mesogenic units aligned in parallel with the direction of the incident light under illumination by the obliquely incident 450 nm visible light for sufficient time. The surface topography of the striping-patterned films was finely recorded with a profilometer, exhibiting periodically raised and depressed areas (Fig. 5d) corresponding to the dark and bright stripes shown in Fig. 5c. The measured height difference of adjacent stripes was 60 ± 3 nm, approximately one-fifth of the total film thickness (~300 nm). Therefore we can not only realize the patterned orientation, but also change the surface roughness of the PNB-Azo-100 thin film through photoalignment only by modulating the incident direction of the visible light, which shows obvious advantages and is significantly different from the conventional rubbing-mediated aligning process. Moreover, the reversible photoalignment and orientation erasure of the striping-patterned surfaces can be repeated many times such as the POM image periodic changes for 5 cycles are presented in Fig. S11. The excellent "writing" and "erasing" capabilities of PNB-Azo-100 thin films without noticeable fatigue were highly fascinating for the fabrication of responsive smart surfaces with desirable structures.

### 3.6. Fabrication of a two-domain LC cell device based on photoaligned PNB-Azo-100 thin film as command surface

Fabrication of LC cells with independent multi-domain alignments was carried out based on PNB-Azo-100 thin films as command surface to direct the orientation of non-photoresponsive LC molecules [41–43]. A two-domain PNB-Azo-100 thin film on ITO-coated glass was fabricated through illumination successively with vertically (Fig. 6a), then 45° incident of 450 nm visible light (Fig. 6b). Afterwards, two pieces of such two-domain photoaligned ITO-glass were assembled into a cell with about 6 μm gap determined by $SiO_2$ particle spacers (Fig. 6c). The LC mixture E7 ($T_{NI}$ = 59 °C) was injected into the cell through capillary effect at around 65 °C and then slowly cooled down to room temperature (Fig. 6d).

The actual alignment state of the as-prepared LC cell was then monitored with POM observation. Upon rotating the LC cell with respect to the polarizer anticlockwise, there always existed a clear boundary between the left and right regions of different alignment, the left domain exhibited continuous brightness changes while the right part always remained dark as exemplified with evolving POM images every 30° (Fig. 6g–j). The conoscopic POM images varied with the oblique angle for the obliquely oriented domain while remained the same unchanged extinction black cross texture for the vertically oriented region further confirmed the oblique or vertical photoalignments of the PNB-Azo-100 thin film and their command surface effect for the upper layer E7 liquid crystals (see Fig. S12). Thus it was revealed that the alignment information of Azo chromophores in the two-domain photoaligned PNB-Azo-100 thin film has been exactly transferred to the non-photoresponsive nematic LC mixture E7 through command surface effect with the LC molecules in the left region of the LC cell aligned in an oblique direction (Fig. 6e) and those in the right region in vertical orientation (Fig. 6f). However, in our attempts to fabricate two-domain aligned LC cells based on PNB-Azo-50 thin films in the same preparation protocol, unfortunately, it turned out that the pre-aligned low-DP azopolynorbornene thin film was partially dissolved by the LC mixture of E7, showing an almost uniform fine grainy POM texture without region difference (Fig. S13). Therefore, combining excellent photoresponsive

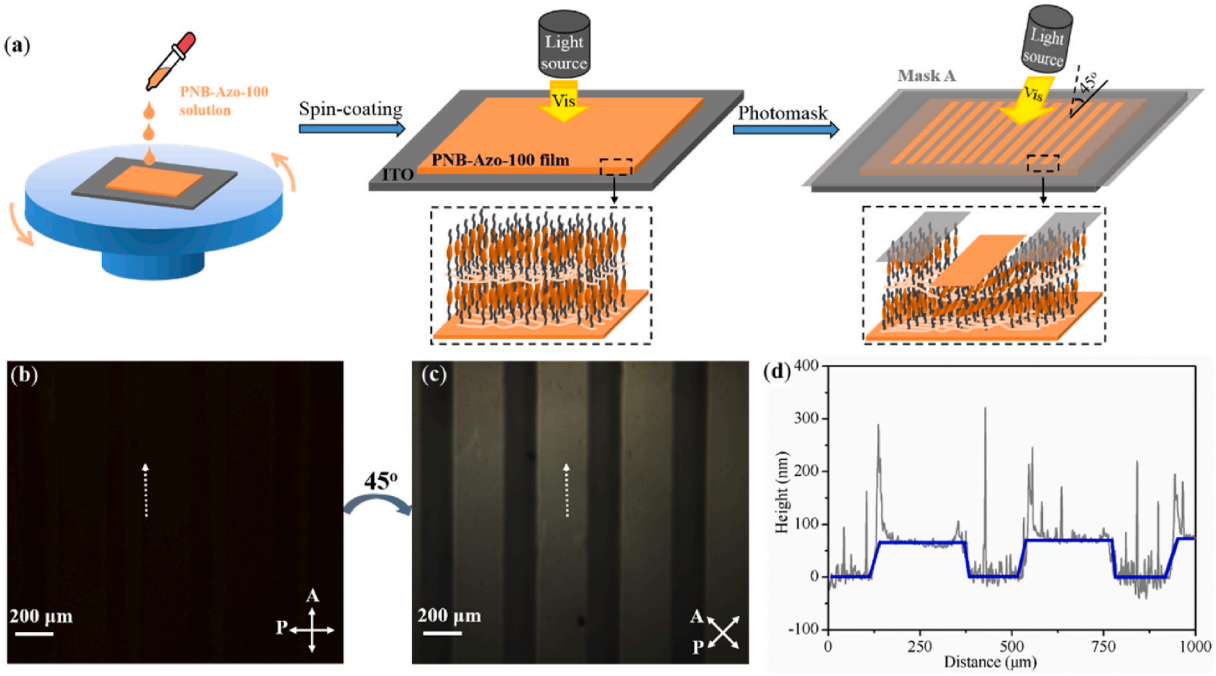


**Fig. 5.** (a) Schematic illustration of the periodic striping pattern formation on the surface of spin-coated PNB-Azo-100 thin films under illumination with 450 nm visible light vertically and then 45° obliquely incident through a banded grating mask A, with enlarged cartoon insets showing the alignment of the azobenzene chromophores. POM images of striping-patterned films with the projection of the obliquely incident light as indicated with a white dashed arrow at an angle of (b) 0°, or (c) 45° to the polarizer direction. P: polarizer, A: analyzer. (d) Surface height profile of thus prepared striping-patterned films measured with a profilometer at room temperature.

characteristics with good compatibility and dissolution-resistance to the nematic LC mixture of E7, the high-DP azopolynorbornene of PNB-Azo-100 was chosen for the fabrication of command surface thin films.

### *3.7. Demonstrating selectively optically readable patterned LC writings based on photoaligned command surface of PNB-Azo-100 thin film*

As shown in Fig. 7a, illumination with the vertically incident 450 nm visible light for sufficient time to ensure a complete homeotropic orientation throughout the PNB-Azo-100 thin film to produce the azopolymer command surface #1 (marked as C1) on ITO-coated conductive glass denoted as ITO-C1. With the incident direction of the 450 nm visible light adjusted to an oblique angle of 30° to the substrate with its projection direction in parallel to y axis, the command surface ITO-C2 was produced with obliquely aligned "NJU" region from ITO-C1 through a mask C with hollowed-out letters of "NJU" (Fig. 7b). Then ITO-C2 was subsequently irradiated with 365 nm UV light through the combination of mask B with mask C to trigger the *trans-cis* photoisomerization of Azo units in "N" region to produce the command surface of ITO-C3 (Fig. 7c). With ITO-C1 and ITO-C3, respectively, as the upper and bottom interior surfaces, a LC cell with about 6 μm gap was assembled, after filling with the LC mixture E7 and slowly cooled down to room temperature, a LC cell written with selectively optically readable "NJU" letters was fabricated (Fig. 7d).

When the projection direction of the obliquely oriented "JU" letters was at an angle of 45° to the polarizer (Fig. 7e), all the three letters "NJU" could be clearly observed and read out. Upon rotating the LC cell by an angle of 45°, the letters "JU" disappeared while "N" remained visible and readable (Fig. 7f). Such selectively optically readable writings reflected visually different orientation states of the E7 LC molecules, which was commanded by the photoaligned PNB-Azo-100 thin films. Specifically, with the POM dark field of view exhibited by the homeotropically oriented LC serving as the black background, the E7 LC molecules in the letters of "JU" regions adopted an oblique orientation induced by the obliquely photoaligned PNB-Azo-100 command surface and showed a visible or vanishing change with the rotating direction change. While due to induced disturbance of the *cis*-isomer of azobenzene resulted from the *trans-cis* photoisomerization under 365 nm UV illumination, the LC molecules in the letter "N" region were in a non-alignment state and always visible under POM. The realization of selectively optically readable writings based on PNB-Azo-100 thin film mediated LC cells manifested that such kind of high-DP azopolynorbornenes with good film-forming characteristic and efficient *trans-cis* photoisomerization capability served as excellent orientation directing materials, which are highly desirable and promising for the fabrication of readable and erasable optical data storage devices in modern information system for document security or anti-forgery and smart card technology.

### *3.8. Checkerboard patterns formation by digital micromirror device (DMD) based dynamic photoalignment*

The digital micromirror device (DMD) based microlithography system as schematically illustrated in Fig. 8a can serve as a kind of dynamic masks, which can produce arbitrary patterns through individually tilting angle control of each micromirror, thus provide a one-mask-for-all method capable of generating complex patterns with great ease, avoiding the cost inefficiency, arduousness and inevitable registration issue based on conventional amplitude multiple-mask method, as well as the resolution limitation due to the beam expansion [60]. As shown in Figs. 8a, upon 450 nm visible light illumination with the incident direction at an angle of 60° to the surface firstly transformed the thin film into obliquely aligned in parallel to the direction of the incident light similar to that demonstrated in Fig. 5. Then, the obliquely aligned film was placed on the carrier stage of DMD system and exposed to the collimated beam reflected by the dynamic photomask in a pre-programmed pattern to induce homeotropic orientation of Azo chromophores in exposed areas. It is worth mentioning that the time required for the DMD photoaligning process was only within seconds, which has benefited both from the excellent photoresponsiveness of

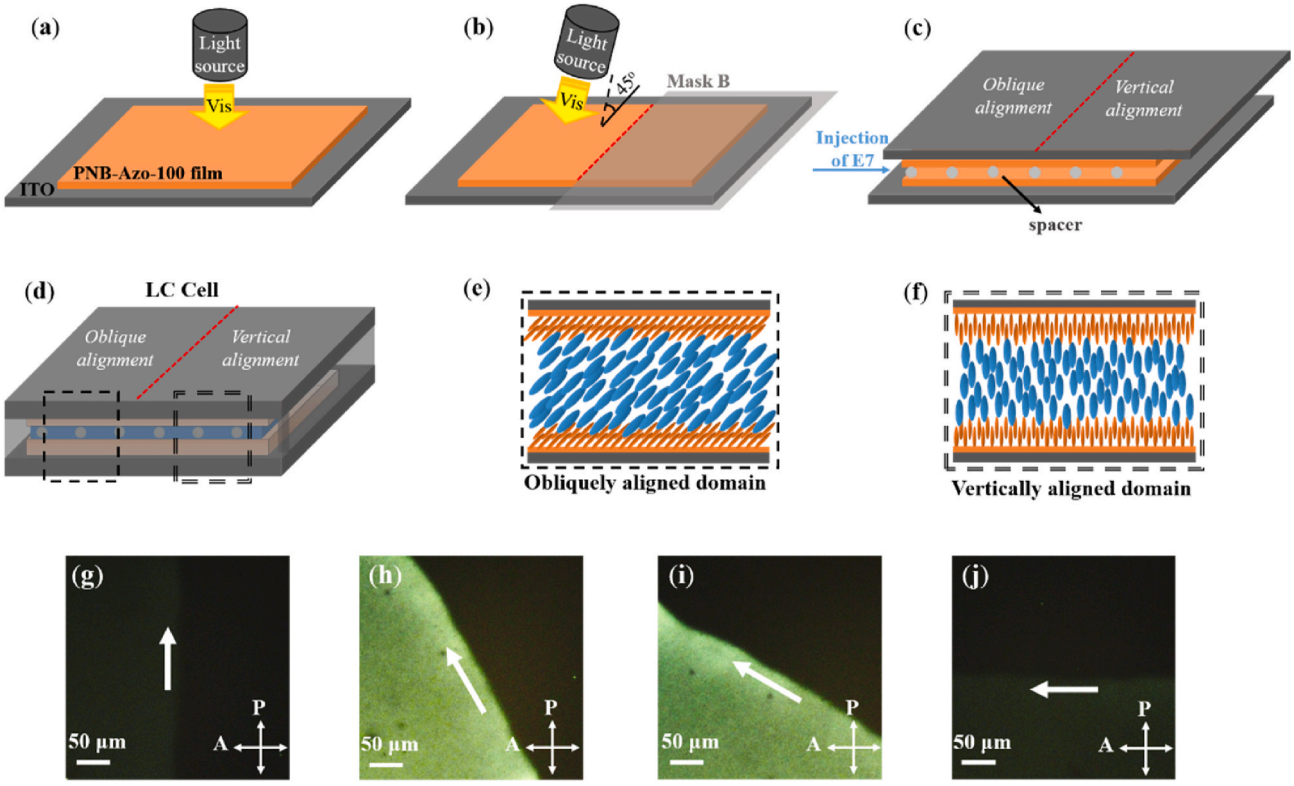


**Fig. 6.** Demonstration of a two-domain LC cell based on command surface effect of photoaligned PNB-Azo-100 thin films. (a) Vertical photoalignment of the PNB-Azo-100 thin film spin-coated on ITO substrate by the vertically incident 450 nm visible light. (b) Half area oblique alignment of the pre-aligned film through a mask B by a 45° incident 450 nm visible light with the obliquely incident light projection in parallel with the dashed red dividing line. (c) Injection of the nematic LC mixture E7 into the assembled cell through capillary effect. (d) Schematic structure of the integrated LC cell with the left and right parts in (e) oblique alignment and (f) vertical alignment, respectively. POM image changes of the LC cell with the projection direction of the obliquely orientated domains at an angle of (g) 0°, (h) 30°, (i) 60°, (j) 90° to the polarizer. P: polarizer, A: analyzer. Scale bar: 50 μm. The one-way white arrow indicating the projection of the obliquely aligned direction. (For interpretation of the references to colour in this figure legend, the reader is referred to the Web version of this article.)

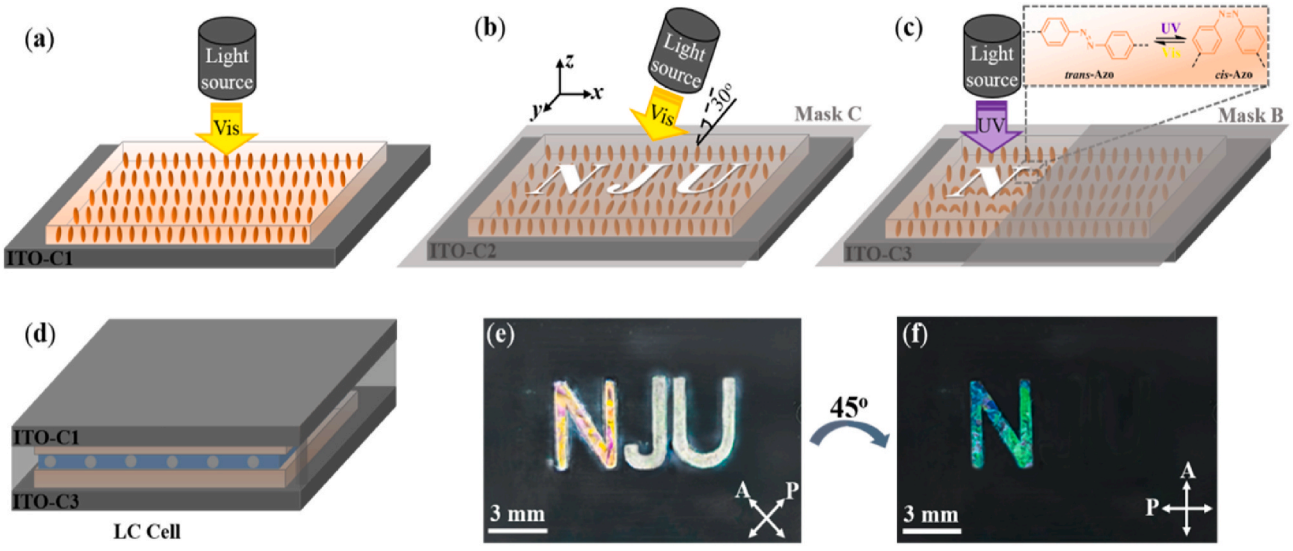


**Fig. 7.** Demonstration of selectively optically readable LC writings mediated by photoaligned PNB-Azo-100 thin films as the command surface. (a) Vertical orientation of a PNB-Azo-100 thin film spin-coated on ITO-glass substrate by the vertically incident 450 nm visible light to produce ITO-C1. (b) Selective oblique orientation induced by a 30° obliquely incident 450 nm visible light through a mask C with letters of "NJU" on ITO-C1 to produce ITO-C2. (c) Triggering *trans-cis* photoisomerization with 365 nm UV light irradiation through both the mask B and mask C to produce ITO-C3. (d) Filling the nematic LC mixture E7 into the LC cell sandwiched between ITO-C1 and ITO-C3 with gap around 6 μm. POM images of "NJU" imprinted LC cell with the projection direction of the obliquely oriented "JU" letters at an angle of (e) 45°, and (f) 90° to the polarizer. P: polarizer, A: analyzer. Scale bar: 3 mm.

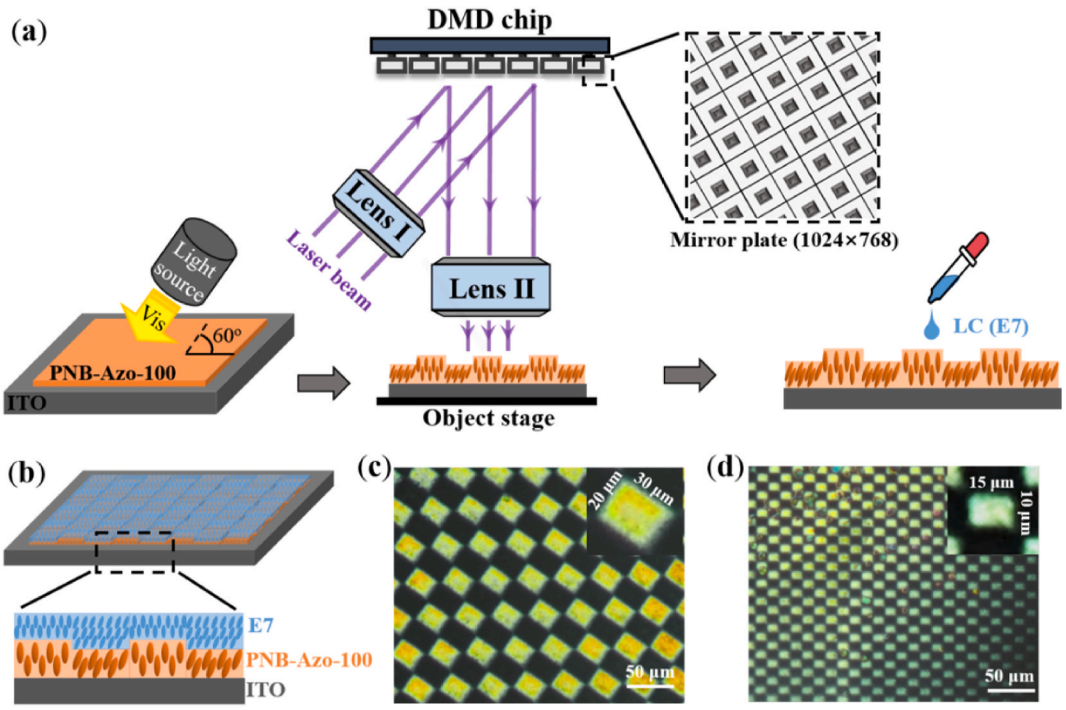


**Fig. 8.** (a) Checkerboard patterns fabrication with the DMD lithography system based on programmable photopatterned PNB-Azo-100 thin films functioning as command surface to direct the orientation of E7 LC molecules spin-coated on the upper layer. (b) Schematic illustration of the preparation of E7/azopolymer on ITO-glass substrate. POM images of the checkerboard with an approximate grid resolution of (c) 30 × 20 μm, and (d) 15 × 10 μm. Lens I: Collimating lens; Lens II: Objective lens set. Scale bar: 50 μm.

PNB-Azo-100 thin film and the high energy of the adopted laser beam.

Upon finishing the photoalignment process with the DMD technique, the photopatterned PNB-Azo-100 thin films were functioned as the command surface to direct the orientation of the non-photoresponsive LC molecules such as E7, which were successively spin-coated as the upper layer (Fig. 8b). As shown in Fig. 8c, the checkerboard pattern with good contrast manifested that the photoalignment information of the PNB-Azo-100 thin film was successfully transferred to the upper layer non-photoresponsive E7 with the bright and black grid images corresponding to the obliquely and vertically orientated regions, respectively. As each micromirror in the digital mirror plate could be set in On/Off state independently through computer programming, the grid resolution of the checkerboard pattern could be further enhanced by subdividing the number of micromirrors in each On/Off domain, which was difficult or impossible to achieve *via* the conventional photomask-based photoaligning process. A checkerboard pattern with higher grid resolution up to sub-ten micrometer could be achieved as demonstrated in Fig. 8d. The successful realization of the checkerboard pattern in ultra-high imaging quality also reflected the sufficient chemical stability and structural reproducibility of the photoaligned PNB-Azo-100 thin films to resist the possible damage caused by the laser light irradiation. More exquisite and fascinating patterns or complex devices can be anticipated based on such kind of azopolynorbornene thin films photoaligned by the advanced DMD micro-lithography system, which are highly desirable for LC photoalignment system and responsive devices and some further work is underway.

## 4. Conclusion

In summary, two azobenzene side-chain LC polynorbornenes of PNB-Azo-n with different DP of $n = 50$ and 100 have been well synthesized through ROMP. The polynorbornene backbone of less flexibility with larger spacing between adjacent side groups endowed stronger inhibition for azobenzene H-aggregation and better photoresponsiveness. The comparative study on the thermal properties and packing structures of azopolynorbornenes of different DP provided reasonable justifications and molecular level understanding for the better performance of high-DP polymer PNB-Azo-100 in photoisomerization and photoalignment. Together with its good compatibility and dissolution-resistance to the nematic LC mixture of E7, the high-DP azopolynorbornene of PNB-Azo-100 was chosen for the fabrication of command surface thin films. The PNB-Azo-100 thin films well behaved as photoalignment regulated command surface for the upper layer nematic LC molecules, enabling selectively optically readable LC graphic writings at normal size through various photomasks or even reaching higher grid resolution up to sub-ten micrometer with a DMD based dynamic photopatterning system, demonstrating promising applications in LC photoalignment system and photoresponsive devices for potential anti-forgery document security and smart card technology.

## CRediT authorship contribution statement

**Jian Chen:** Methodology, Investigation, Formal analysis, Writing - original draft. **Tianchi Xu:** Investigation, Validation, Writing - review & editing. **Weiguang Zhao:** Investigation, Writing- original draft. **Ling-Ling Ma:** Investigation, Formal analysis, Writing - review & editing. **Dongzhong Chen:** Conceptualization, Methodology, Supervision, Funding acquisition, Writing - review & editing. **Yan-Qing Lu:** Supervision, Resources, Funding acquisition.

## Declaration of competing interest

The authors declare that they have no known competing financial interests or personal relationships that could have appeared to influence the work reported in this paper.

## Acknowledgements

This work was supported by the National Natural Science Foundation of China (Grants No.21875098, 21574062, and 52003115), the Natural

Science Foundation of Jiangsu Province (BK20200320) and also partially by Program for Changjiang Scholars and Innovative Research Team in University (IRT_16R38), and the Fundamental Research Funds for the Central Universities and the Scientific Research Foundation of Graduate School of Nanjing University (Grant 2017ZDL06). We thank Prof. Wei Hu for his kind help in the DMD system and inspiring discussions.

## Appendix B. Supplementary data

Supplementary data to this article can be found online at https://doi.org/10.1016/j.polymer.2021.123492.

## References

[1] J.A. Delaire, K. Nakatani, Linear and nonlinear optical properties of photochromic molecules and Materials, Chem. Rev. 100 (2000) 1817–1845.
[2] F. Ercole, T.P. Davis, R.A. Evans, Photo-responsive systems and biomaterials: photochromic polymers, light-triggered self-assembly, surface modification, fluorescence modulation and beyond, Polym. Chem. 1 (2010) 37–54.
[3] S. Lee, H.S. Kang, J.-K. Park, Directional photofluidization lithography: micro/nanostructural evolution by photofluidic motions of azobenzene materials, Adv. Mater. 24 (2012) 2069–2103.
[4] H.K. Bisoyi, Q. Li, Light-driven liquid crystalline materials: from photo-induced phase transitions and property modulations to applications, Chem. Rev. 116 (2016) 15089–15166.
[5] X. Li, R. Wen, Y. Zhang, Li Zhu, B. Zhang, H. Zhang, Photoresponsive side-chain liquid crystalline polymers with an easily cross-linkable azobenzene mesogen, J. Mater. Chem. 19 (2009) 236–245.
[6] S. Jiang, Y. Zhao, L. Wang, L. Yin, Z. Zhang, J. Zhu, W. Zhang, X. Zhu, Photocontrollable induction of supramolecular chirality in achiral side chain Azo-containing polymers through preferential chiral solvation, Polym. Chem. 6 (2015) 4230–4239.
[7] M.C. Spiridon, K. Aissou, M. Mumtaz, C. Brochon, E. Cloutet, G. Fleury, G. Hadziioannou, Surface relief gratings formed by microphase-separated disperse red 1 acrylate-containing diblock copolymers, Polymer 137 (2018) 378–384.
[8] K. Ichimura, Photoalignment of liquid-crystal systems, Chem. Rev. 100 (2000) 1847–1874.
[9] A. Natansohn, P. Rochon, Photoinduced motions in azo-containing polymers, Chem. Rev. 102 (2002) 4139–4176.
[10] T. Ikeda, Photomodulation of liquid crystal orientations for photonic applications, J. Mater. Chem. 13 (2003) 2037–2057.
[11] C.J. Barrett, J. Mamiya, K.G. Yager, T. Ikeda, Photo-mechanical effects in azobenzene-containing soft materials, Soft Matter 3 (2007) 1249–1261.
[12] H. Akiyama, T. Kawara, H. Takada, H. Takatsu, V. Chigrinov, E. Prudnikova, V. Kozenkov, H. Kwok, Synthesis and properties of azo dye aligning layers for liquid crystal cells, Liq. Cryst. 29 (2002) 1321–1327.
[13] L. Ma, S. Li, W. Li, W. Ji, B. Luo, Z. Zheng, Z. Cai, V. Chigrinov, Y. Lu, W. Hu, Rationally designed dynamic superstructures enabled by photoaligning cholesteric liquid crystals, Adv. Optical Mater. 3 (2015) 1691–1696.
[14] J.-W. Weener, E.W. Meijer, Photoresponsive dendritic monolayers, Adv. Mater. 12 (2000) 741–746.
[15] E. Blasco, J.L. Serrano, M. Pinol, L. Oriol, Light responsive vesicles based on linear-dendritic block copolymers using azobenzene−aliphatic codendrons, Macromolecules 46 (2013) 5951–5960.
[16] K. Ichimura, S.K. Oh, M. Nakagawa, Light-driven motion of liquids on a photoresponsive surface, Science 288 (2000) 1624–1626.
[17] S.-K. Oh, M. Nakagawa, K. Ichimura, Relationship between the ability to control liquid crystal alignment and wetting properties of calix[4]resorcinarene monolayers, J. Mater. Chem. 11 (2001) 1563–1569.
[18] S. Pan, M. Ni, B. Mu, Q. Li, X. Hu, C. Lin, D. Chen, L. Wang, Well-defined pillararene-based azobenzene liquid crystalline photoresponsive materials and their thin films with photomodulated surfaces, Adv. Funct. Mater. 25 (2015) 3571–3580.
[19] W. Jo, J. Choi, H.S. Kang, M. Kim, S. Baik, B.J. Lee, C. Pang, H.T. Kim, Programmable fabrication of submicrometer bent pillar structures enabled by a photoreconfigurable azopolymer, ACS Appl. Mater. Interfaces 12 (2020) 5058–5064.
[20] Z. Wu, T. Xu, D. Chen, Fabrication of re-shapeable liquid crystalline elastomers with dynamic C-N bonds and investigation of their reversible photoresponsive bending behaviors, Sci. Sin. Chim. 50 (2020) 620–630.
[21] S. Sun, S. Liang, W. Xu, G. Xu, S. Wu, Photoresponsive polymers with multi-azobenzene groups, Polym. Chem. 10 (2019) 4389–4401.
[22] X. Pang, J. Lv, C. Zhu, L. Qin, Y. Yu, Photodeformable azobenzene-containing liquid crystal polymers and soft actuators, Adv. Mater. (2019), 1904224.
[23] J. Tian, L. Fu, Z. Liu, H. Geng, Y. Sun, G. Lin, X. Zhang, G. Zhang, D. Zhang, Optically tunable field effect transistors with conjugated polymer entailing azobenzene groups in the side chains, Adv. Funct. Mater. 29 (2019), 1807176.
[24] J. Wang, Y. Zheng, L. Li, E. Liu, C. Zong, J. Zhao, J. Xie, F. Xu, T.A.F. Konig, M. Grenzer Saphiannikova, Y. Cao, A. Fery, C. Lu, All-optical reversible azo-based wrinkling patterns with high aspect ratio and polarization-independent orientation for light-responsive soft photonics, ACS Appl. Mater. Interfaces 11 (2019) 25595–25604.
[25] C. Zong, M. Hu, U. Azhar, X. Chen, Y. Zhang, S. Zhang, C. Lu, Smart copolymer-functionalized flexible surfaces with photo-switchable wettability: from superhydrophobicity with "rose petal" effect to superhydrophilicity, ACS Appl. Mater. Interfaces 11 (2019) 25436–25444.
[26] J. Royes, A. Nogales, T.A. Ezquerra, L. Oriol, R.M. Tejedor, M. Piñol, Effect of the polymer architecture on the photoinduction of stable chiral organizations, Polymer 143 (2018) 58–68.
[27] K. Wang, L. Yin, T. Miu, M. Liu, Y. Zhao, Y. Chen, N. Zhou, W. Zhang, X. Zhu, Design and synthesis of a novel azobenzenecontaining polymer both in the main- and side-chain toward unique photocontrolled isomerization properties, Mater. Chem. Front. 2 (2018) 1112–1118.
[28] J. Lv, Y. Liu, J. Wei, E. Chen, L. Qin, Y. Yu, Photocontrol of fluid slugs in liquid crystal polymer microactuators, Nature 537 (2016) 179.
[29] Z. Chen, Y.-T. Chan, D. Miyajima, T. Kajitani, A. Kosaka, T. Fukushima, J.M. Lobez, T. Aida, A design principle of polymers processable into 2D homeotropic order, Nat. Commun. 7 (2016), 13640.
[30] T. Takeshima, W. Liao, Y. Nagashima, K. Beppu, M. Hara, S. Nagano, T. Seki, Photoresponsive surface wrinkle morphologies in liquid crystalline polymer films, Macromolecules 48 (2015) 6378–6384.
[31] D. Wang, X. Wang, Amphiphilic azo polymers: molecular engineering, self-assembly and photoresponsive properties, Prog. Polym. Sci. 38 (2013) 271–301.
[32] A. Ambrosio, L. Marrucci, F. Borbone, A. Roviello, P. Maddalena, Light-induced spiral mass transport in azo-polymer films under vortex-beam illumination, Nat. Commun. 3 (2012) 989.
[33] N. Hosono, T. Kajitani, T. Fukushima, K. Ito, S. Sasaki, M. Takata, T. Aida, Large-area three-dimensional molecular ordering of a polymer brush by one-step processing, Science 330 (2010) 808–811.
[34] T. Ikeda, O. Tsutsumi, Optical switching and image storage by means of azobenzene liquid-crystal films, Science 268 (1995) 1873–1875.
[35] Y. Morikawa, S. Nagano, K. Watanabe, K. Kamata, T. Iyoda, T. Seki, Optical alignment and patterning of nanoscale microdomains in a block copolymer thin film, Adv. Mater. 18 (2006) 883–886.
[36] H. Yu, T. Iyoda, T. Ikeda, Photoinduced alignment of nanocylinders by supramolecular cooperative motions, J. Am. Chem. Soc. 128 (2006) 11010–11011.
[37] H. Yu, S. Asaoka, A. Shishido, T. Iyoda, T. Ikeda, Photoinduced nanoscale cooperative motion in a well-defined triblock copolymer, Small 3 (2007) 768–771.
[38] H. Yu, T. Ikeda, Photocontrollable liquid-crystalline actuators, Adv. Mater. 23 (2011) 2149–2180.
[39] H. Yu, Recent advances in photoresponsive liquid-crystalline polymers containing azobenzene chromophores, J. Mater. Chem. C 2 (2014) 3047–3054.
[40] T. Wang, X. Li, Z. Dong, S. Huang, H. Yu, Vertical orientation of nanocylinders in liquid-crystalline block copolymers directed by light, ACS Appl. Mater. Interfaces 9 (2017) 24864–24872.
[41] K. Ichimura, Y. Suzuki, T. Seki, A. Hosoki, K. Aoki, Reversible change in alignment mode of nematic liquid crystals regulated photochemically by command surfaces modified with an azobenzene monolayer, Langmuir 4 (1988) 1214–1216.
[42] K. Aoki, T. Seki, Y. Suzuki, T. Tamaki, A. Hosoki, K. Ichimura, Factors affecting photoinduced alignment regulation of cyclohexanecarboxylate-type nematic liquid crystals by azobenzene molecular films, Langmuir 8 (1992) 1007–1013.
[43] Kunihiro Ichimura, Molecular amplification of photochemical events, J. Photochem. Photobiol. Chem. 158 (2003) 205–214.
[44] S. Furumi, M. Kidowaki, M. Ogawa, Y. Nishiura, K. Ichimura, Surface-mediated photoalignment of discotic liquid crystals on azobenzene polymer films, J. Phys. Chem. B 109 (2005) 9245–9254.
[45] S. Furumi, K. Ichimura, Surface-assisted photoalignment of discotic liquid crystals by nonpolarized light irradiation of photo-cross-linkable polymer thin films, J. Phys. Chem. B 111 (2007) 1277–1287.
[46] T. Seki, M. Sakuragi, Y. Kawanishi, Y. Suzuki, T. Tamaki, R. Fukuda, K. Ichimura, "Command surfaces" of Langmuir-Blodgett films. photoregulations of liquid crystal alignment by molecularly tailored surface azobenzene layers, Langmuir 9 (1993) 211–218.
[47] T. Seki, K. Ichimura, R. Fukuda, T. Tanigaki, T. Tamaki, Illumination-induced modifications of Langmuir-Blodgett films consisting of a deuterated poly(vinyl alcohol) having an azobenzene side chain transferred at varied packing density, Macromolecules 29 (1996) 892–898.
[48] T. Seki, Mono- and multilayers of photoreactive polymers as collective and active supramolecular systems, Supramol. Sci. 3 (1996) 25–29.
[49] T. Seki, T. Fukuchi, K. Ichimura, Humidity sensitive characteristic stacking of azobenzene in monolayer of urea amphiphile on hydrophilic surface, Langmuir 16 (2000) 3564–3567.
[50] T. Ubukata, T. Seki, K. Ichimura, Modeling the interface region of command surface 1. Structural evaluations of azobenzene/liquid crystal hybrid Langmuir monolayers, J. Phys. Chem. B 104 (2000) 4141–4147.
[51] T. Ubukata, T. Seki, S. Morino, K. Ichimura, Modeling the interface region of command surface 2. Spectroscopic evaluations of azobenzene/liquid crystal hybrid Langmuir-Blodgett films under illumination, J. Phys. Chem. B 104 (2000) 4148–4154.
[52] K. Fukuhara, S. Nagano, M. Hara, T. Seki, Free-surface molecular command systems for photoalignment of liquid crystalline materials, Nat. Commun. 5 (2014) 3320.
[53] T. Nakai, D. Tanaka, M. Hara, S. Nagano, T. Seki, Free surface command layer for photoswitchable out-of-plane alignment control in liquid crystalline polymer films, Langmuir 32 (2016) 909–914.

[54] D.Y. Kim, S. Shin, W.J. Yoon, Y.J. Choi, J.K. Hwang, J.S. Kim, C.R. Lee, T.L. Choi, K.U. Jeong, From smart denpols to remote-controllable actuators: hierarchical superstructures of azobenzene-based polynorbornenes, Adv. Funct. Mater. 27 (2017) 1606294.
[55] H.A. Haque, S. Kakehi, M. Hara, S. Nagano, T. Seki, High-density liquid-crystalline azobenzene polymer brush attained by surface-initiated ring-opening metathesis polymerization, Langmuir 29 (2013) 7571–7575.
[56] R.H. Lambeth, J.S. Moore, Light-induced shape changes in azobenzene functionalized polymers prepared by ring-opening metathesis polymerization, Macromolecules 40 (2007) 1838–1842.
[57] M.V. Bermeshev, P.P. Chapala, Addition polymerization of functionalized norbornenes as a powerfultool for assembling molecular moieties of new polymers withversatile properties, Prog. Polym. Sci. 84 (2018) 1–46.
[58] M. Wu, M. Gong, D. Zhou, R. Wang, D. Chen, Effect of grafting density on the self-assembly of side-chain discotic liquid crystalline polymers with triphenylene discogens, Soft Matter 16 (2020) 375–382.
[59] X. Li, Q. Li, Y. Wang, Y. Quan, D. Chen, Y. Cheng, Strong aggregation-induced CPL response promoted by chiral emissive nematic liquid crystals (N*-LCs), Chem. Eur J. 24 (2018) 12607–12612.
[60] H. Wu, W. Hu, H. Hu, X. Lin, G. Zhu, J.W. Choi, V. Chigrinov, Y. Lu, Arbitrary photo-patterning in liquid crystal alignments using DMD based lithography system, Optic Express 20 (2012) 16684–16689.
[61] B. Wei, W. Hu, Y. Ming, F. Xu, S. Rubin, J. Wang, V. Chigrinov, Y. Lu, Generating switchable and reconfigurable optical vortices via photopatterning of liquid crystals, Adv. Mater. 26 (2014) 1590–1595.
[62] L. Ma, S. Wu, W. Hu, C. Liu, P. Chen, H. Qian, Y. Wang, L. Chi, Y. Lu, Self-assembled asymmetric microlenses for four-dimensional visual imaging, ACS Nano 13 (2019) 13709–13715.